11th International Workshop on Ship and Marine Hydrodynamic
Hamburg, Germany, September 22-25, 2019

Numerical Study of Sloshing Motion on Unstructured Mesh Using UMTHINC

Mohamed M. Kamra[1,*], Changhong Hu[1]

[1]Kyushu University, Research Institute for Applied Mechanics
6-1 Kasuga-koen, Kasuga, 816-8580, JAPAN

[*]Corresponding author, mohamed.kamra@riam.kyushu-u.ac.jp

ABSTRACT

The numerical simulations of sloshing motions are performed for different test cases with various filling levels and oscillation frequencies. The numerical results are analyzed and compared with experimental data. The numerical computations are performed with a Volume Of Fluid (VOF) based Reynolds-Averaged Navier-Stokes (RANS) solver. Our in-house numerical solver employs the unstructured multi-dimensional tangent hyperbolic interface capturing method (UMTHINC) for free-surface capturing combined with various turbulence models. The sloshing motion is numerically modeled using the body-force method which introduces a source term into the momentum equation corresponding to the tank motion profile.

The numerical results of impact pressure and free-surface are compared with published experimental data wherever possible. The effect of turbulence model choice on loading predictions is highlighted by studying several RANS models and analyzing its effect on fluid motion and impact pressure. The effect of tank internal structures is studied by considering two approaches: finite thickness approach and zero-thickness approach. The developed solver is able to accurately capture the complex interface structure without smearing even with long time integration. The results showed a favorable agreement of impact pressure as well as the general fluid motion.

1 INTRODUCTION AND BACKGROUND

In hydrodynamics, sloshing is defined as the fluid motion which occurs when a partially filled container undergoes external excitation. An important result of such motions is the dynamic pressure loads on the container structure, which constitutes a problem for offshore structure design and especially important for LNG carriers. Generally, sloshing flows are considered strongly non-linear, in-homogeneous, and three-dimensional. Sloshing loads are significantly affected by violent flow phenomena such as impact, wave breaking, and splashes. Experimental studies have been widely used to get a better understanding of such flows, however, it is often difficult to correctly scale all the physics involved and extend the obtained results to full scale. Moreover, experimental studies require a huge amount of time, and effort to carry out relatively simple cases with simplified geometries[1, 2]. To overcome such difficulties, numerical simulations are widely used in the evaluation of sloshing loads.

The most popular approach for simulating tank sloshing problems is the solution of the Navier-Stokes equations using finite difference, finite volume or more recently finite element discretization methods. A suitable method for treating the moving interface(free surface) is employed to handle the multi-fluid system.

Sloshing motion can be modeled as laminar or turbulent. Due to the comparatively good numerical stability and low computational cost of laminar models, it has usually been preferred and used in many

sloshing studies[3–5]. In these studies, the results were compared to results obtained using turbulent models and concluded that liquid turbulence effect on free surface profiles and impact pressure is insignificant and can be neglected. On the contrary, other studies[2, 6, 7] showed significant variation when comparing laminar solutions to solutions obtained using turbulence models. The results concluded that the turbulence effect should be taken into account when simulating sloshing flows.

Recent works of the numerical simulation of sloshing flows can be summarized as follows. A comparison of the laminar approach with the turbulent approach, conducted using the Reynolds averaged Navier-Stokes equations (RANS) model, Large eddy simulations(LES), and very large eddy simulations (VLES), has been performed by Liu et al.[8]. The study showed that the inclusion of a turbulence model is essential to the numerical prediction of sloshing flows. The choice of the turbulence model also plays a critical role in obtaining accurate numerical solutions. Sufyan et al.[9] applied a dynamic mesh-adaptation algorithm based on an unstructured mesh to solve sloshing problems by a finite element method. The study showed that dynamic adaption can reduce the computational cost by at least half. However, the relative mass error was not negligible when the base grid resolution was insufficient.

Next, we review the different methods that could be used to treat the free surface. The most popular ones are the volume of fluid (VOF) methods and the level-set methods.

Level set methods use the signed distance function to track the interface identified by the zero level-set contour. The method provides improved accuracy in curvature computation for surface tension dominated flows as well as the easy application of the boundary conditions at the interface as in the case of single-phase free surface flows. Level set methods are quite simple, accurate and easy to implement which makes it very attractive for many CFD developers. However, such methods don't guarantee mass/volume conservation thus causing the disappearance of tiny droplets. Many improvements were introduced to treat this issue by applying re-distancing/re-initialization of the level set field [10], introducing conservation formulation or simply coupling the method with a VOF method [11, 12]. Although most level set methods are developed for Cartesian meshes, a few recent attempts were made to extend the method to unstructured meshes[13–16].

In the volume of fluid (VOF) methods, first introduced by Hirt and Nichols[17], a volume fraction field α ranging between zero and one is introduced. The volume fraction signifies the ratio of the volume of fluid in a computational cell so it serves as a means of identifying each fluid in the field. The time evolution of the volume fraction field is governed by the advection equation $\frac{D\alpha}{Dt} = 0$. VOF methods are classified into two main categories:

- Geometric based methods[13, 18–24] that require geometric reconstruction of the interface which makes the underlying geometrical and computational complexity quite substantial, especially on unstructured grids.
- Algebraic methods[25–27] which are in principle based on finite volume advection schemes thus it is more appealing for implementation on unstructured grids.

Following a different approach than other algebraic methods, the tangent hyperbolic interface capturing (THINC) was proposed by Xiao et al.[28]. The THINC methods utilize a tangent hyperbolic function to reconstruct the volume fraction field. The methods provide a conservative advection scheme in which interface jump thickness can be controlled and maintained throughout the time evolution by a single parameter. The method was originally proposed for uniform Cartesian grids[29, 30] but it was later successfully extended to unstructured triangular and tetrahedral meshes [31] and quadrilateral and hexahedral meshes Xie et al.[32] and the method was designated as Unstructured Multi-dimensional THINC (UMTHINC). Following that, a formulation for prismatic and pyramid cells was introduced[33] making the method fully applicable to all cell shapes in unstructured meshes. The quality of the results produced by the method was quite competitive with other VOF methods with hardly any complexity during implementation on unstructured meshes. Most recently, the method was reformulated for quadratic interface profiles thus substantially improving the accuracy without a significant increase in computational cost. The new method was designated THINC with Quadratic surface representation and Gaussian quadrature Xie and Xiao[34] (THINC/QQ).

The present article is organized as follows: the governing equations and numerical method are described in the following section. Then, a description of the model problem and computational grid used in this work is provided followed by the validation and case results discussion. Finally, some concluding remarks on improvements and further research are made.

2 GOVERNING EQUATIONS AND NUMERICAL METHOD

The numerical computations were carried using the in-house developed computational fluid dynamics code based on the finite-volume discretization of the incompressible Navier-Stokes equations. The Reynolds averaging approach is applied to the Navier-Stokes equations for turbulence modeling, as a result, the Reynolds Averaged Navier Stokes (RANS) equations can be written in Cartesian tensor form as

$$\frac{\partial \bar{u}_i}{\partial x_i} = 0 \tag{1}$$

$$\rho(\frac{\partial \bar{u}_i}{\partial t} + \frac{\partial(\bar{u}_i\bar{u}_j)}{\partial x_j}) = \rho g_i - \rho\frac{dU_i}{dt} + \frac{\partial}{\partial x_j}(-\bar{P}\delta_{ij} + (\mu+\mu_t)(\frac{\partial \bar{u}_i}{\partial x_j} + \frac{\partial \bar{u}_j}{\partial x_i})) \tag{2}$$

where x_i is the position component in Cartesian coordinates, $\bar{u}_i$ is the time-averaged velocity component, ρ is the fluid density, $\bar{P}$ is the time-averaged static pressure, g_i is the gravity acceleration component, U_i is the translational velocity component of the tank fixed coordinate, μ is the molecular viscosity, and μ_t is the turbulent eddy viscosity. To ensure balance for the external force, the piezometric pressure variable is defined following the work of Montazeri and Ward[35], as $p = P - \rho\vec{g}\cdot\vec{x} + \rho\frac{d\vec{U}}{dt}\cdot\vec{x}$ where p is the piezometric pressure. Thus, rewriting the momentum equation;

$$\rho(\frac{\partial \bar{u}_i}{\partial t} + \frac{\partial(\bar{u}_i\bar{u}_j)}{\partial x_j}) = \frac{\partial}{\partial x_j}\left(-\bar{p}\delta_{ij} - g_k x_k\bar{\rho}\delta_{ij} + \frac{dU_k}{dt}x_k\bar{\rho}\delta_{ij} + (\mu+\mu_t)(\frac{\partial \bar{u}_i}{\partial x_j} + \frac{\partial \bar{u}_j}{\partial x_i})\right) \tag{3}$$

It should be noted that the surface tension term is omitted due to its limited effect in body force dominated flows.

In the present work, three turbulence models are employed for turbulence closure in the RANS approach; Standard $k-\epsilon$ model, Realizable $k-\epsilon$ model, and Wilcox $k-\omega$ model.

Standard $k-\epsilon$ model This model is the most common RANS models to simulate the mean flow characteristics for turbulent flow conditions. In the standard $k-\epsilon$ model the turbulent eddy viscosity μ_t is defined as

$$\mu_t = \rho C_\mu \frac{k^2}{\epsilon} \tag{4}$$

where k is the kinetic energy of turbulence and ϵ is the dissipation rate of turbulence kinetic energy. The transport equations for the model are given by

$$\rho(\frac{\partial k}{\partial t} + \frac{\partial(k\bar{u}_j)}{\partial x_j}) = \frac{\partial}{\partial x_j}\left((\mu + \frac{\mu_t}{\sigma_k})\frac{\partial k}{\partial x_j}\right) + P_k - \rho\epsilon \tag{5}$$

$$\rho(\frac{\partial \epsilon}{\partial t} + \frac{\partial(\epsilon\bar{u}_j)}{\partial x_j}) = \frac{\partial}{\partial x_j}\left((\mu + \frac{\mu_t}{\sigma_\epsilon})\frac{\partial \epsilon}{\partial x_j}\right) + C_{\epsilon 1}\frac{\epsilon}{k}P_k - C_{\epsilon 2}\rho\frac{\epsilon^2}{k} \tag{6}$$

Realizable $k-\epsilon$ model This model is considered an improvement on the standard model and provides better predictions for flows involving rotation, boundary layers under strong adverse pressure gradients, separation and re-circulation. In the realizable $k-\epsilon$ model, the turbulent eddy viscosity μ_t is defined using Equation (4) however C_μ is not constant but calculated from the formula presented by Shih et al.[36]. The $k-$equation for this model is the same as the standard model and only the ϵ-equation is different and it is given by

$$\rho(\frac{\partial \epsilon}{\partial t} + \frac{\partial(\epsilon\bar{u}_j)}{\partial x_j}) = \frac{\partial}{\partial x_j}\left((\mu + \frac{\mu_t}{\sigma_\epsilon})\frac{\partial \epsilon}{\partial x_j}\right) + \rho\, C_1 S\epsilon - \rho\, C_2\frac{\epsilon^2}{k+\sqrt{\nu\epsilon}} + C_{1\epsilon}\frac{\epsilon}{k}C_{3\epsilon}P_b + S_\epsilon \tag{7}$$

Wilcox $k-\omega$ model In the $k-\omega$ model the turbulent eddy viscosity μ_t is defined as

$$\mu_t = \rho\frac{k}{\omega} \tag{8}$$

where k is the kinetic energy of turbulence and ω is the specific dissipation rate of turbulence kinetic energy. The transport equations for this model are given by

$$\rho(\frac{\partial k}{\partial t} + \frac{\partial(k\bar{u}_j)}{\partial x_j}) = \frac{\partial}{\partial x_j}\left((\mu + \alpha_k\mu_t)\frac{\partial k}{\partial x_j}\right) + P_k - \beta^*\rho k\omega \tag{9}$$

$$\rho(\frac{\partial \omega}{\partial t} + \frac{\partial(\omega\bar{u}_j)}{\partial x_j}) = \frac{\partial}{\partial x_j}\left((\mu + \alpha_\omega\mu_t)\frac{\partial \omega}{\partial x_j}\right) + \gamma\frac{\omega}{k}P_k - \beta\rho\omega^2 \tag{10}$$

In this work, the volume of fluid method is used for the time evolution of the free surface. In the VOF method, different fluids are assigned each an indicator (color) function $C(x,t)$ which has a value of one inside the fluid and zero otherwise. Discretely, the volume fraction α is defined as the volume average of the indicator function over the computational cell.

$$\alpha = \frac{1}{|\Omega_i|}\oint_{\Omega_i} C(\vec{x},t)\, d\Omega \tag{11}$$

The one-fluid model is adopted in this work. Therefore, the material properties in the fluid are updated based on the volume fraction as

$$\rho = \rho_1\alpha + (1-\alpha)\rho_2 \quad \text{and} \quad \mu = \mu_1\alpha + (1-\alpha)\mu_2 \tag{12}$$

where $\rho_{1,2}$ and $\mu_{1,2}$ are the density and viscosity properties of fluids 1 and 2 respectively. The time evolution of the volume fraction equation is governed by the following advection equation.

$$\frac{\partial\alpha}{\partial t} + \nabla\cdot(\alpha\vec{V}) = \alpha\nabla\cdot\vec{V} \tag{13}$$

The UMTHINC scheme is employed for the treatment of the free surface. The method ensures sharp interface at the free surface while maintaining simple and efficient implementation even for hybrid unstructured grids[32–34, 37]. In the THINC method, the interface jump is defined as a smoothed piecewise hyperbolic tangent profile, so the indicator function is now approximated as

$$C(\vec{x}) = \frac{1}{2}\Big(1 + tanh\left(\beta(P(\vec{x}) + d)\right)\Big) \tag{14}$$

where β is the sharpness parameter which controls how steep(thin) is the interface region between the two fluids. The interface surface equation is defined by $P(x) + d = 0$ where $P(x)$ is a polynomial with coefficients based on the interface geometric characteristics such as the unit normal vector $\vec{n} = (n_x, n_y, n_z)$ and curvature matrix I_{xyz} of the interface. In this work, only linear interface reconstruction is considered.

In this work, the three-dimensional incompressible turbulent flow is solved using the non-iterative time advancement Pressure-Implicit with Splitting of Operator (PISO) algorithm with 4 neighbor correction and one non-orthogonality correction steps during each time step to ensure that both the continuity and momentum equations are satisfied. For more details on this method, the reader is referred to references [38]. Second order three level time implicit scheme was applied for the time discretization of the momentum equation. The second order Total Variation Diminishing(TVD) limited linear upwind scheme was used for the convection term with the Sweby limiter[39]. The cell-based Green-Gauss gradient method was used to compute the velocity and pressure gradients. The previously mentioned computational parameters were set based on the authors' experience from previous numerical studies which are not reported here.

The presented RANS models constitute a generic transport equation in the field variable ϕ as follows

$$\underbrace{\frac{\partial \phi}{\partial t}}_{\text{Temporal term}} + \underbrace{\nabla \cdot (\rho \vec{V} \phi)}_{\text{Convection Term}} = \underbrace{\nabla \cdot \left(\Gamma \nabla \phi\right)}_{\text{Diffusion Term}} + \underbrace{S_\phi}_{\text{Source}} \tag{15}$$

The treatment of the temporal, convection, and diffusion term is conducted in a manner similar to the momentum equation. However, in turbulence field equations, the source terms can either be treated implicitly or explicitly. The convention[40] is that the source term is treated implicitly when it has a negative sign so it would contribute to the improvement of the stability and convergence of the underlying linear system of equations by increasing the matrix's diagonal dominance. For the same reason, a source term is treated explicitly if it has a positive sign.

The finite volume formulation of the volume fraction equation method is written as

$$\frac{\partial \alpha_i}{\partial t} = -\sum_{j=1}^{J} v_{n_{ij}} \alpha_{ij} |\Delta S_{ij}| + \alpha_i \sum_{j=1}^{J} v_{n_{ij}} |\Delta S_{ij}| \tag{16}$$

where j is the j^{th} face of cell Ω_i, α_{ij} is the face value of the volume fraction, $|\Delta S_{ij}|$ is the face area, and $v_{n_{ij}}$ is the normal velocity on the face.
The numerical method used to implement UMTHINC can be summarized in the following steps:

1. The calculation of interface unit normal vector $\vec{n} = (n_x, n_y, n_z)$ at the cell-center
2. The calculation of unknown d such that Equation (11) is satisfied.
3. The calculation of the volume fraction face value α_{ij}.
4. Advancing the volume fraction equation in time.

In the current study, the interface unit normals are computed using the node averaged least square Gauss (NAG) method. The methods used to compute the unknown d and face value of the volume fraction α_{ij} are explained, in detail, in ref[31, 32, 34]. The third order explicit Runge-Kutta TVD (RK3)[41, 42] is used to advance the volume fraction equation Equation (16) in time.

3 MODEL PROBLEM AND COMPUTATIONAL GRID

In the present study, two model problems are considered; the first is for the purpose of validation and examination of the numerical method while the second is for demonstration and further discussions. In both model problems, water and air at 20°C were selected as the liquid and gas in the rectangular tank, respectively. The experiments conducted by the National Maritime Research Institute of Japan was chosen for validation[43]. The rectangular tank used in these experiments has a length $L = 1.2m$, a height $H = 0.6m$ and a width $W = 0.2m$. During the experiment, it was confirmed that the flow can be considered to be two-dimensional (2D) therefore only 2D simulations will be considered in this work. Pressure sensors at 14 locations were used in the experiments to measure the pressure time evolution on the side, bottom and top walls of the tank. In this work, the pressure data from only two sensors P_2, and P_3 were considered due to the low filling level (20% of the tank height) used in the experiments. The tank origin is placed in the centroid of the tank and the locations of the two pressure sensors are clearly shown in Figure 1. It should be noted that only the pure sway motion (translation in x-axis) was considered in the present study. The sway amplitude A=0.06m and two cases for the period; the first has a period $T = 1.74s$ and the second has a period T=1.94s referred to as case A and case B respectively.

For demonstration purposes, we modify the current model by introducing a vertical baffle with a thickness of 6mm at $x = 0$ and a height flushing with the free surface. The effect of the vertical baffle on the reduction of impact pressure is examined. The numerical treatment of the baffle is also investigated

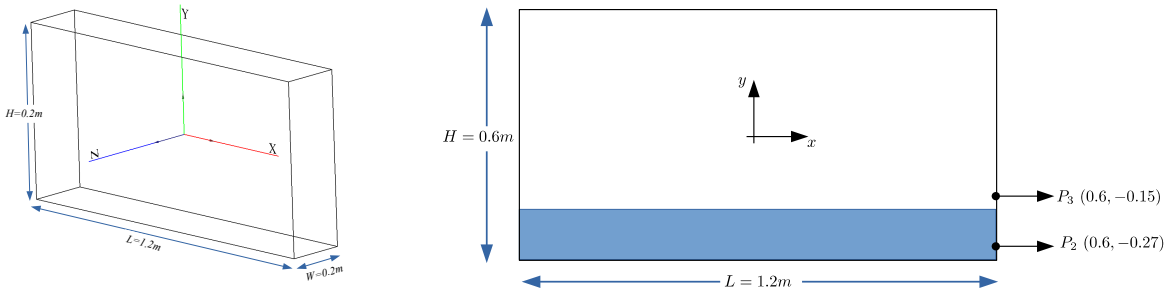

Figure 1: Geometry and pressure sensor locations for the rectangular tank sway case [43, 44]

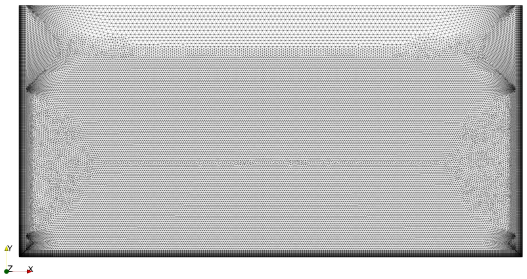

Figure 2: A 2D unstructured grid for the validation test case

by considering the finite thickness(actual case) approach and the zero thickness (shell) approach on the numerical accuracy and computational efficiency of the solution. Despite the possibility of using structured grids for this test case, a 2D hybrid unstructured grid was generated to assess the accuracy and efficiency of the developed in-house code. In the generated grid, 20 quadrilateral layers are attached to the walls of the tank, with a first layer thickness of 0.5mm, to accurately resolve the boundary layer. Triangular cells are used for the remaining region of the domain, as shown in Figure 2. During grid generation, attention is directed to the general region around the free surface to ensure accurate resolution of the interface.

4 VALIDATION AND DISCUSSION

In this section, we first examine the effect of the turbulence model on the accuracy of the computed solution. The case with the shorter motion period, case A where $T = 1.74s$, was chosen for this since it represents a more violent case. Based on the examination results, the chosen turbulence model is used for all remaining test cases. It should be noted that in the following results, the UMTHINC sharpness parameter β was set to 6. This choice is based on many numerical studies and experiments which emphasize on temporal numerical stability while maintaining high accuracy and sharp interface capturing[37].

First, the effect of turbulence model choice on the accuracy of the numerical results is investigated. Examination of the governing equation for the three RANS models considered in this work shows that the realizable $k-\epsilon$ is slightly more computationally expensive than the other two models. This can be attributed to the additional computations necessary to evaluate C_μ in Equation (4) which are given in ref[36].

In Figure 3, the turbulence fluctuation field, defined as the square root of the turbulence kinetic energy $\sqrt{k}$, is examined for the three RANS models at the same time instant. The thick black line in each figure represents the free surface profile. Both the standard $k-\epsilon$ and the Wilcox $k-\omega$ models give a fairly similar free surface profile. However, the realizable $k-\epsilon$ model predicts a lower wave climb height and an air pocket at the impact. Further, it also predicts high turbulence fluctuation localized near the nose of the wave with more turbulence on the air side of the free surface. In the standard $k-\epsilon$ model, the turbulence fluctuation seems more diffused in the air side with the Wilcox $k-\omega$ model giving even higher turbulence fluctuation fields in both water and air.

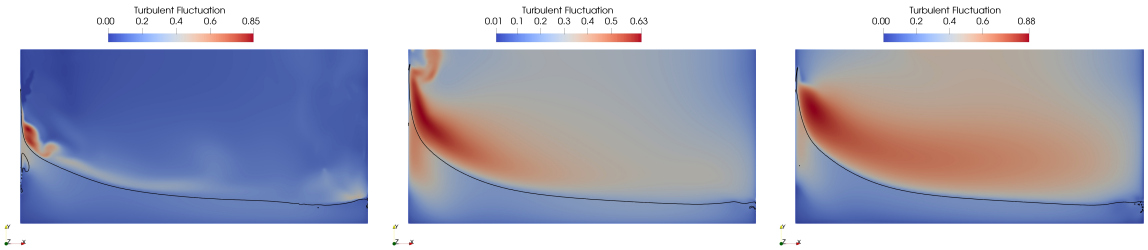

Figure 3: A comparison of the turbulent fluctuation field for the realizable $k-\epsilon$ model (left), standard $k-\epsilon$ (middle), and Wilcox $k-\omega$ model (right)

Examination of the pressure time-history depicted in Figure 4 confirms our previous findings and shows that the realizable $k-\epsilon$ model gives a shorter impact duration when compared to the other models. The Wilcox $k-\omega$ model and standard $k-\epsilon$ model give very close predictions with the $k-\omega$ model being more accurate when compared to experimental data. Based on these results, the $k-\omega$ model is used Case B.

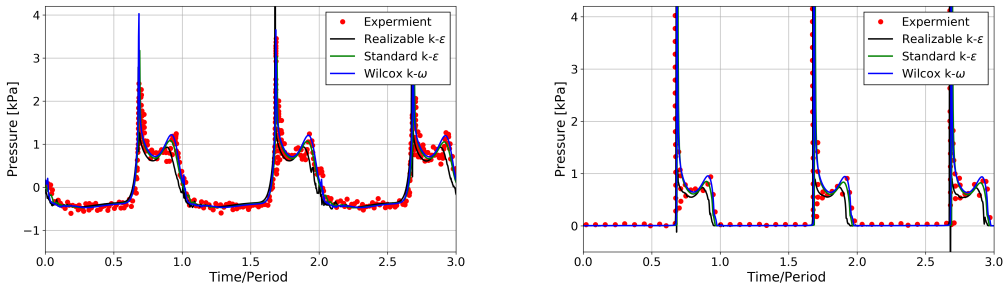

Figure 4: A comparison of the turbulent fluctuation field for realizable $k-\epsilon$ model, standard $k-\epsilon$, and Wilcox $k-\omega$ model for P_2 (left), and P_3 (right)

For case B, Figure 5 shows the instantaneous free surface profile from the numerical simulation when compared with experimental video snapshots at approximately the same time instant within the motion cycle(period). The agreement is very good in terms of the general free surface shape.

Figure 6 shows a comparison of the pressure time-history with the experimental data. The overall qualitative and quantitative agreement is very good especially for the two pressure spikes where the first spike represents the sloshing liquid impacting the side wall and the second spike represent the sloshing liquid collapsing after it had climbed the wall.

5 TANK SLOSHING WITH VERTICAL BAFFLES

In this section, we further demonstrate the capability of the developed by introducing a 6mm vertical baffle at the center line of the rectangular tank. The excitation motion used in this test case has an amplitude of 0.06m and a period of 1.94s. The results are then compared to a zero-thickness approximate baffle model thus highlighting the effect of baffle thickness on the sloshing flow. Two unstructured grid are generated in a manner similar the validation case. The baffle is also fitted with 20 quadrilateral layers to provide accurate resolution of the boundary layers as shown in Figure 7. The grid for the finite thickness baffle case is comprised of 108.8K cells while the approximate shell baffle case is nearly 101.65K cells for nearly identical grid resolution over the domain. The shell baffle model allows for simpler grid generation even with complex internal structure cases. It further allows for easier implementation of flexible baffle cases where baffle displacement/deflection can be done by simply perturbing the vertices coinciding on the baffle and its surrounding layers thus avoiding grid regeneration and providing some performance

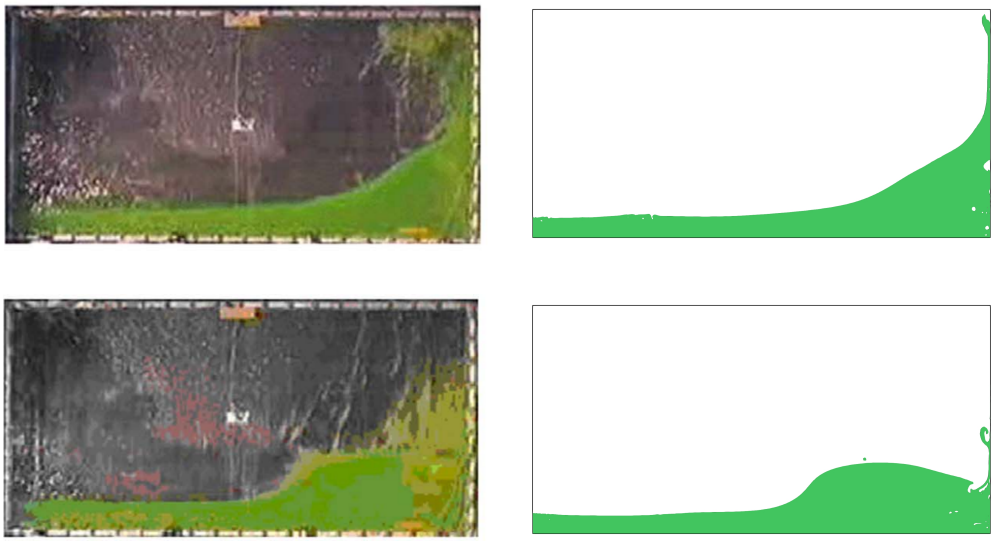

Figure 5: Comparison of the 2D free surface profile from the experiment(left) and numerical simulations(right) at selected time instants for case B

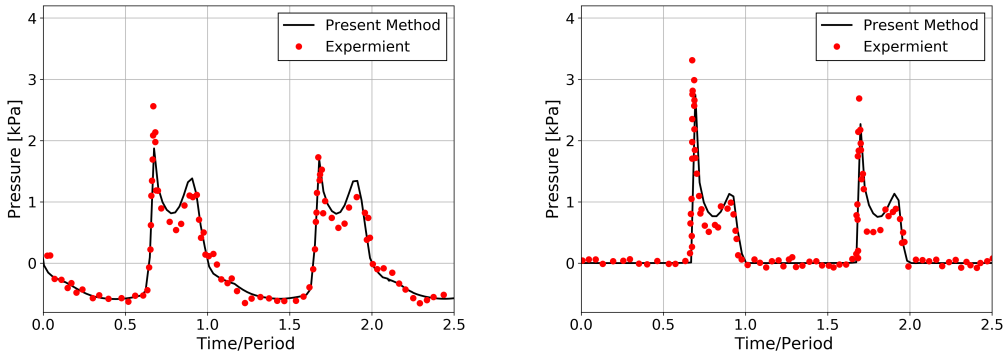

Figure 6: Comparison of the pressure time-history at P_2(left), and P_3(right) for case B

savings.

In Figure 8, a comparison of the pressure field for the two baffle cases as well as the free surface depicted by a thick black contour line is presented. The figure shows very similar behavior in the region surrounding the baffle where significant air pockets and bubbles are observed. Although the free surface profile seems qualitatively similar, a clear difference in the static pressure field is observed between the two cases. The shell baffle case seems to significantly over-predict the pressure field especially in the region of the wall that is being impacted by the wave.

Further examining the pressure time-history given by Figure 9, it is clear that, as expected, the vertical baffle has significantly suppressed the impact pressure at the side wall. The figure also shows the shell baffle approximation gives 50% higher impact pressure than the finite thickness case. Phase difference is also observed in the pressure time evolution between the two considered approaches. In order to explain this numerical behavior, it is necessary to compute more test cases for larger and smaller thickness baffles with the shell baffle case being a limiting/asymptotic case.

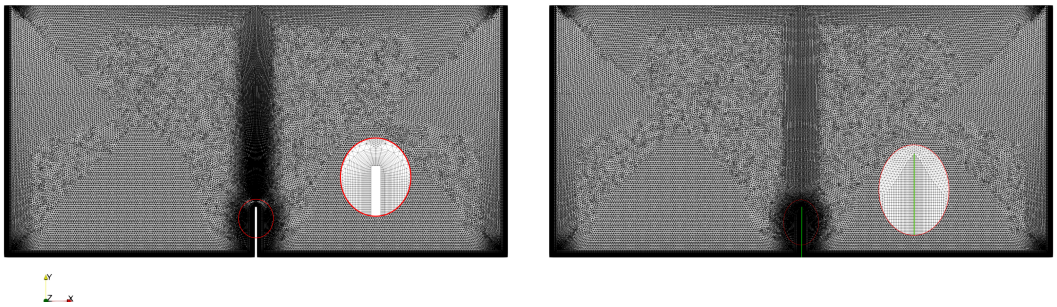

Figure 7: A 2D unstructured grid for the finite thickness case (left), and zero thickness case (right)

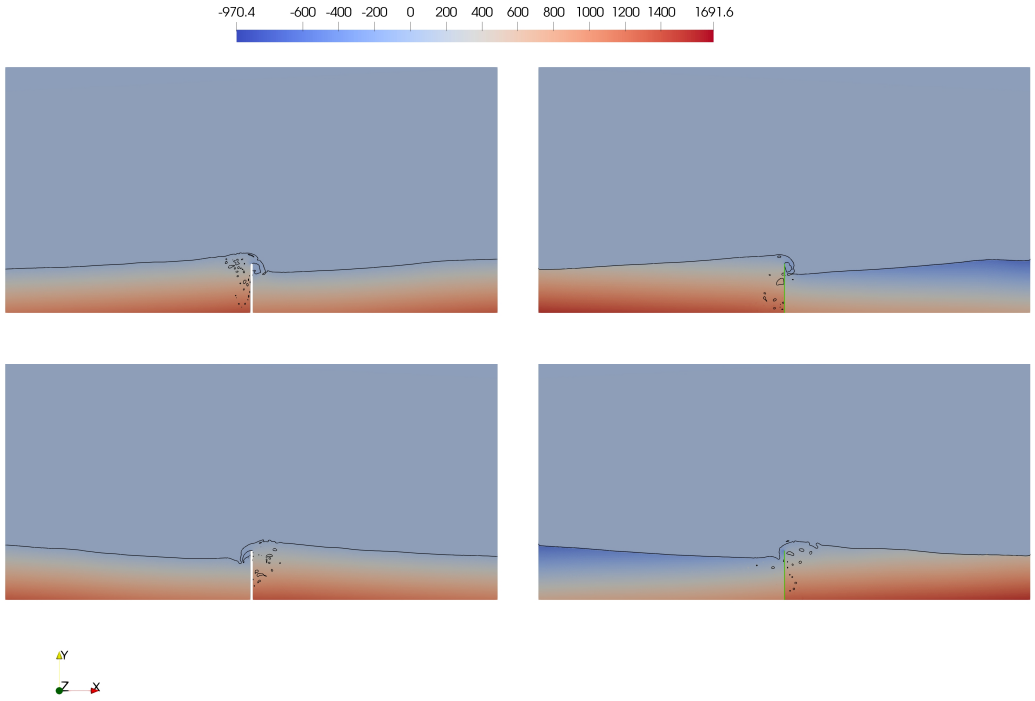

Figure 8: Comparison of the pressure field for the finite thickness case (left), and zero thickness case (right) at selected time instants

6 CONCLUSION

A description of our newly developed two-phase turbulent flow solver based on UMTHINC method has been presented. The UMTHINC method ensures sharp interface at the free surface while maintaining simple and efficient implementation even for hybrid unstructured grids. Examining several RANS turbulence models confirms non-negligible turbulent fluctuations in both water and air. Although all turbulence models give fairly good agreement for the pressure time-history with experiment data, the $k-\omega$ model was found to give the best matching. The numerical results were validated against experimental data thus demonstrating very good agreement both qualitatively and quantitatively. As expected, introducing a vertical baffle to rectangular tank managed to significantly suppress the pressure impacts, especially the peaks, on the tank walls. Although the approximate shell baffle approach was able to qualitatively give a similar free surface profile as the finite thickness baffle approach, significant difference were observed for the pressure prediction which warrants additional investigations. Important issues for future research include further investigation of the baffle thickness on the predicted pressure, modeling air compressibility and the buffer effect of bubbles and air pockets on load predictions.

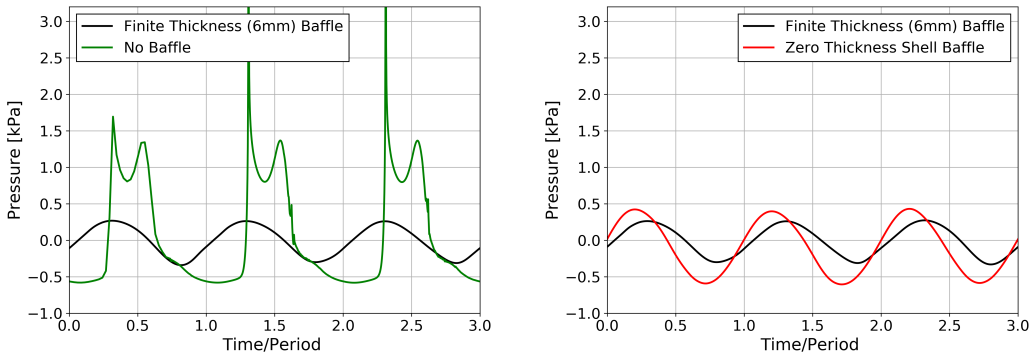

Figure 9: Comparison of the pressure time-history on the sidewall at P_2 for the finite thickness baffle case and no-baffle/bare case (left), and zero thickness shell baffle case (right)

REFERENCES

[1] L. Delorme, A. Colagrossi, A. Souto-Iglesias, R. Zamora-Rodriguez and E. Botia-Vera. "A set of canonical problems in sloshing, Part I: Pressure field in forced roll-comparison between experimental results and SPH". In: *Ocean Engineering* 36.2 (2009), pp. 168–178.

[2] B. Godderidge. "A phenomenological rapid sloshing model for use as an operator guidance system on liquefied natural gas carriers". PhD thesis. University of Southampton, 2009.

[3] S. Aliabadi, A. Johnson and J. Abedi. "Comparison of finite element and pendulum models for simulation of sloshing". In: *Computers & fluids* 32.4 (2003), pp. 535–545.

[4] L. Khezzar, A. Seibi and A. Goharzadeh. "Water sloshing in rectangular tanks–an experimental investigation & numerical simulation". In: *International Journal of Engineering (IJE)* 3.2 (2009), p. 174.

[5] K. Modaressi-Tehrani, S. Rakheja and I. Stiharu. "Three-dimensional analysis of transient slosh within a partly-filled tank equipped with baffles". In: *Vehicle System Dynamics* 45.6 (2007), pp. 525–548.

[6] S. H. Rhee. "Unstructured grid based Reynolds-averaged Navier-Stokes method for liquid tank sloshing". In: *Journal of fluids engineering* 127.3 (2005), pp. 572–582.

[7] T. M. Wasfy, J. O'Kins and S. Smith. "Experimental validation of a time-accurate finite element model for coupled multibody dynamics and liquid sloshing". In: *SAE Transactions* (2007), pp. 10–25.

[8] D. Liu, W. Tang, J. Wang, H. Xue and K. Wang. "Comparison of laminar model, RANS, LES and VLES for simulation of liquid sloshing". In: *Applied Ocean Research* 59 (2016), pp. 638–649.

[9] M. Sufyan, L. C. Ngo and H. G. Choi. "A dynamic adaptation method based on unstructured mesh for solving sloshing problems". In: *Ocean Engineering* 129 (2017), pp. 203–216.

[10] M. Sussman and E. Fatemi. "An efficient, interface-preserving level set redistancing algorithm and its application to interfacial incompressible fluid flow". In: *SIAM Journal on scientific computing* 20.4 (1999), pp. 1165–1191.

[11] M. Sussman and E. G. Puckett. "A coupled level set and volume-of-fluid method for computing 3D and axisymmetric incompressible two-phase flows". In: *Journal of computational physics* 162.2 (2000), pp. 301–337.

[12] Y.-Y. Tsui, C.-Y. Liu and S.-W. Lin. "Coupled level-set and volume-of-fluid method for two-phase flow calculations". In: *Numerical Heat Transfer, Part B: Fundamentals* 71.2 (2017), pp. 173–185.

[13] N. Balcázar, O. Lehmkuhl, L. Jofre, J. Rigola and A. Oliva. "A coupled volume-of-fluid/level-set method for simulation of two-phase flows on unstructured meshes". In: *Computers & Fluids* 124 (2016), pp. 12–29.

[14] M. Dianat, M. Skarysz and A. Garmory. "A Coupled Level Set and Volume of Fluid method for automotive exterior water management applications". In: *International Journal of Multiphase Flow* 91 (2017), pp. 19–38.

[15] Z. Cao, D. Sun, B. Yu and J. Wei. "A coupled volume-of-fluid and level set (VOSET) method based on remapping algorithm for unstructured triangular grids". In: *International Journal of Heat and Mass Transfer* 111 (2017), pp. 232–245.

[16] Z. Cao, D. Sun, J. Wei and B. Yu. "A coupled volume-of-fluid and level set method based on multi-dimensional advection for unstructured triangular meshes". In: *Chemical Engineering Science* 176 (2018), pp. 560–579.

[17] C. W. Hirt and B. D. Nichols. "Volume of fluid (VOF) method for the dynamics of free boundaries". In: *Journal of computational physics* 39.1 (1981), pp. 201–225.

[18] D. L. Youngs. "Time-dependent multi-material flow with large fluid distortion". In: *Numerical methods for fluid dynamics* (1982).

[19] B. Parker and D. Youngs. *Two and three dimensional Eulerian simulation of fluid flow with material interfaces*. Atomic Weapons Establishment, 1992.

[20] J. Lopez, J. Hernandez, P. Gomez and F. Faura. "An improved PLIC-VOF method for tracking thin fluid structures in incompressible two-phase flows". In: *Journal of Computational Physics* 208.1 (2005), pp. 51–74.

[21] M. Rudman. "Volume-tracking methods for interfacial flow calculations". In: *International journal for numerical methods in fluids* 24.7 (1997), pp. 671–691.

[22] K. Ito, T. Kunugi, H. Ohshima and T. Kawamura. "A volume-conservative PLIC algorithm on three-dimensional fully unstructured meshes". In: *Computers and Fluids* 88 (2013), pp. 250–261.

[23] T. Maric, H. Marschall and D. Bothe. *voFoam - A geometrical Volume of Fluid algorithm on arbitrary unstructured meshes with local dynamic adaptive mesh refinement using OpenFOAM*. 2013.

[24] L. Jofre, O. Lehmkuhl, J. Castro and A. Oliva. "A 3-D Volume-of-Fluid advection method based on cell-vertex velocities for unstructured meshes". In: *Computers and Fluids* 94 (2014), pp. 14–29.

[25] O. Ubbink. "Numerical prediction of two fluid systems with sharp interfaces". PhD thesis. University of London PhD Thesis, 1997.

[26] D. Zhang, C. Jiang, D. Liang, Z. Chen, Y. Yang and Y. Shi. "A refined volume-of-fluid algorithm for capturing sharp fluid interfaces on arbitrary meshes". In: *Journal of Computational Physics* 274 (2014), pp. 709–736.

[27] F. Denner and B. G. van Wachem. "Compressive VOF method with skewness correction to capture sharp interfaces on arbitrary meshes". In: *Journal of Computational Physics* 279 (2014), pp. 127–144.

[28] F. Xiao, Y. Honma and T. Kono. "A simple algebraic interface capturing scheme using hyperbolic tangent function". In: *International Journal for Numerical Methods in Fluids* 48.9 (2005), pp. 1023–1040.

[29] K. Yokoi. "Efficient implementation of THINC scheme: A simple and practical smoothed VOF algorithm". In: *Journal of Computational Physics* 226.2 (2007), pp. 1985–2002.

[30] S. Ii, K. Sugiyama, S. Takeuchi, S. Takagi, Y. Matsumoto and F. Xiao. "An interface capturing method with a continuous function: The THINC method with multi-dimensional reconstruction". In: *Journal of Computational Physics* 231.5 (2012), pp. 2328–2358.

[31] S. Ii, B. Xie and F. Xiao. "An interface capturing method with a continuous function: The THINC method on unstructured triangular and tetrahedral meshes". In: *Journal of Computational Physics* 259 (2014), pp. 260–269.

[32] B. Xie, S. Ii and F. Xiao. "An efficient and accurate algebraic interface capturing method for unstructured grids in 2 and 3 dimensions: The THINC method with quadratic surface representation". In: *International Journal for Numerical Methods in Fluids* 76.12 (2014), pp. 1025–1042.

[33] B. Xie, P. Jin and F. Xiao. "An unstructured-grid numerical model for interfacial multiphase fluids based on multi-moment finite volume formulation and THINC method". In: *International Journal of Multiphase Flow* 89 (2017), pp. 375–398.

[34] B. Xie and F. Xiao. "Toward efficient and accurate interface capturing on arbitrary hybrid unstructured grids: The THINC method with quadratic surface representation and Gaussian quadrature". In: *Journal of Computational Physics* 349 (2017), pp. 415–440.

[35] H. Montazeri and C. Ward. "A balanced-force algorithm for two-phase flows". In: *Journal of Computational Physics* 257 (2014), pp. 645–669.

[36] T.-H. Shih, W. W. Liou, A. Shabbir, Z. Yang and J. Zhu. "A new k-ϵ eddy viscosity model for high reynolds number turbulent flows". In: *Computers & Fluids* 24.3 (1995), pp. 227–238.

[37] M. M. Kamra. "Development of an Unstructured Grid Solver for Complex Wave Impact Problems". PhD thesis. Kyushu University, 2018.

[38] J. H. Ferziger and M. Peric. *Computational Methods for Fluid Dynamics*. Springer Berlin Heidelberg, 2012.

[39] P. K. Sweby. "High resolution schemes using flux limiters for hyperbolic conservation laws". In: *SIAM Journal on Numerical Analysis* 21.5 (1984), pp. 995–1011.

[40] F. Moukalled, L. Mangani and M. Darwish. *The Finite Volume Method in Computational Fluid Dynamics: An Advanced Introduction with OpenFOAM and Matlab*. Fluid Mechanics and Its Applications. Springer International Publishing, 2015.

[41] C.-W. Shu. "Total-variation-diminishing time discretizations". In: *SIAM Journal on Scientific and Statistical Computing* 9.6 (1988), pp. 1073–1084.

[42] S. Gottlieb and C.-w. Shu. *Total variation diminishing Runge-Kutta schemes*. Tech. rep. Mathematics of Computation, 1998.

[43] Y. Tanaka, T. Ando and T. Miyamoto. "Experimental study on sloshing load measured by panel-type pressure gauge". In: Proceedings General meeting of Ship Research Institute, Ship research institute. Tokyo, Japan, 2000.

[44] M. Sufyan, L. C. Ngo and H. G. Choi. "A dynamic adaptation method based on unstructured mesh for solving sloshing problems". In: *Ocean Engineering* 129 (2017), pp. 203–216.